Published in final edited form as:

ChemPhotoChem. 2021 August ; 5(8): 727–734. doi:10.1002/cptc.202100045.

Photophysical Properties of Indocyanine Green in the Shortwave Infrared Region

Emily D. Cosco[a], **Irene Lim**[a], **Ellen M. Sletten**[a]

[a]Dr. E. D. Cosco, I. Lim, Prof. E. M. Sletten Department of Chemistry and Biochemistry, California NanoSystems Institute, University of California, Los Angeles, 607 Charles E. Young Dr. East, Los Angeles, CA 90095 (USA)

Abstract

With the growing development of new contrast agents for optical imaging using near-infrared and shortwave infrared (SWIR) wavelengths, it is essential to have consistent bench-marks for emitters in these regions. Indocyanine green (ICG), a ubiquitous and FDA-approved organic dye and optical imaging agent, is commonly employed as a standard for photophysical properties and biological performance for imaging experiments at these wavelengths. Yet, its reported photophysical properties across organic and aqueous solvents vary greatly in the literature, which hinders its ability to be used as a consistent benchmark. Herein, we measure photophysical properties in organic and aqueous solvents using InGaAs detection (~950–1,700 nm), providing particular relevance for SWIR imaging.

Graphical Abstract

Sletten@chem.ucla.edu .

Conflict of Interest

The authors declare no conflict of interest.

Supporting information for this article is available on the WWW under https://doi.org/10.1002/cptc.202100045

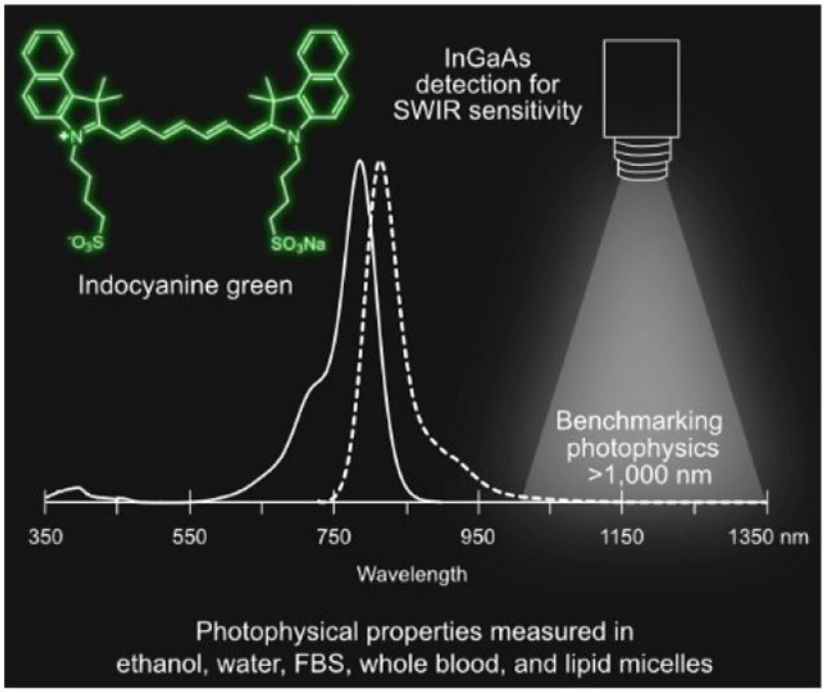

Across the board: Indocyanine green (ICG) is a ubiquitous fluorophore used in fluorescence imaging. We measure its photophysical properties in parallel across ethanol, water, fetal bovine serum (FBS), whole blood, and in a micelle formulation and evaluate performance at SWIR wavelengths. We find that the photophysical behavior of ICG in whole blood and FBS is similar and significantly brighter and more photostable than water, offering an improved benchmark for comparative studies.

Keywords

chromophores; dyes/pigments; imaging agents; near-infrared; photophysical properties

1. Introduction

Indocyanine green (ICG) is a near-infrared (NIR, 700–1,000 nm) polymethine dye widely used as a contrast agent for optical imaging.[1] ICG has been FDA approved for ~60 years and is used pre-clinically and clinically in NIR optical imaging applications, including for angiography,[2] lymphatic,[3–6] biliary[7,8] and intestinal[9] functional imaging, dental imaging,[10] and oncological image guided surgery.[11–13] Additionally, there is increasing interest in broader applications of fluorescence guided surgery[14–17] as well as photoacoustic imaging[18–20] with ICG and ICG conjugates. In 2018, it was reported that ICG has a long wavelength emission tail which extends past the NIR region.[21,22] This property has provided further attention to its use as an imaging agent in the shortwave infrared (SWIR, 1,000–2,000 nm) region (also referred to as NIR-II region). Optical detection in the SWIR region of the electromagnetic spectrum offers increased contrast, resolution, and penetrative properties, compared to detection in the visible (VIS, 350–700 nm) and NIR regions. ICG has proven to be a successful SWIR contrast agent

upon 785 or 808 nm excitation in single channel experiments for vasculature[23,24] and dental[25] imaging, and alongside dyes with more red-shifted absorption properties in multichannel experiments.[26,27] Notably, the SWIR emission of ICG was recently exploited in multispectral image-guided surgery in humans.[28]

Due to ICG's advantageous photophysical properties in biological media, high aqueous solubility, commercial accessibility, validated biological safety and fast hepatic clearance, ICG is a promising contrast agent for the translation of SWIR imaging applications to clinical needs.[25,28] These properties also make ICG a natural benchmark for the development of improved and complementary optical tools for the SWIR region. Indeed, ICG is commonly employed as a comparison for emitters and imaging applications in both the NIR and the SWIR regions.[24,29–38] However, the reported photophysical properties of ICG vary greatly in the literature, resulting in variable and inconsistent comparisons. Further, most previous photophysical measurements were performed on silicon detectors, which lose sensitivity at the NIR and SWIR wavelengths (~ 850–1,100 nm) relevant to the emissive properties of ICG.[39] Photophysical measurements in the literature are provided for reference and comparison in Table S1, where it is evident that many reported values for ICG are in contradiction. There are also few systematic photophysical studies in which both absorptive properties and emissive properties are measured and compared in multiple solvents and biologically relevant media.[40–42]

Here, we measure absorptive and emissive photophysical properties, including absorption and emission spectra, absorption coefficients (ε), fluorescence quantum yields (Φ_F), and photostability for ICG in parallel across five media to enable consistent comparison. These data include measurements in the biological media fetal bovine serum (FBS) and whole blood, and use InGaAs detection for emissive properties, ensuring collection of the full emission spectra of ICG. We evaluate brightness values relevant to SWIR imaging experiments and corroborate the photophysical measurements using SWIR imaging. We aim for these data to be useful in understanding the photophysical behavior of ICG in changing solvent environments and for the establishment of ICG as a comparative benchmark for diverse NIR and SWIR emitters and imaging applications, alike.

2. Results and Discussion

2.1. Photophysical Characterization

The solvents in which we chose to evaluate ICG photophysics are ethanol (EtOH), for an organic solvent reference, and the aqueous media: water, FBS, and whole blood (sourced as sheep's blood due to available quantity and safety). Additionally, we evaluated the photophysical properties of ICG when encapsulated in phospholipid-poly(ethylene)glycol micelles, a common delivery vehicle used for *in vivo* experiments (Figure S1).[43] We chose to omit phosphate buffered saline (PBS), or other solutions with high ionic strengths such as isotonic saline, as we and others[19] have found that these solvents only minimally solubilize ICG as a monomer species. The purity of the ICG sample we used for measurements was verified using ^{1}H NMR (Figures S2–S3). The maximal absorption wavelengths ($\lambda_{max,abs}$), maximal emission wavelengths ($\lambda_{max,em}$), molar absorption coefficient (ε), fluorescence quantum yield (Φ_F) and brightness values calculated from these experimental measurements

are listed in Table 1. Absorption and emission traces obtained in each of these solvents are displayed in Figure 1. Minor red shifts (9–19 nm) of the absorption peak are observed in FBS, micelles, and whole blood as compared to water. These observations are consistent with prior studies.[44–45] We find that the absorption coefficients are all larger than 10^5 $M^{-1}cm^{-1}$, with water as the lowest value at $\varepsilon=1.56\times10^5$ $M^{-1}cm^{-1}$ (see Figure S5). Similar ε values are observed in FBS and micelles in water, while ~1.4-fold improvement is observed over water in EtOH, with $\varepsilon=2.23\times10^5$ $M^{-1}cm^{-1}$. Fluorescence quantum yield measurements also show the lowest values in water, with $\Phi_F=2.9\%$. Micelles in water show minor improvements with $\Phi_F=5.1\%$. In contrast, Φ_F in EtOH, FBS, and whole blood are all similar and considerably higher, between 12–14%. When combining the absorptive and emissive properties together, brightness values (brightness=$\varepsilon\times\Phi_F$) in water are the lowest at 4.5×10^5 $M^{-1}cm^{-1}$. The brightness compared to water is ~2-fold higher in micelles, ~4-fold improved in FBS, and ~79-fold higher in EtOH. The total brightness in blood could not be evaluated photophysically due to high scattering coefficients preventing accurate absorption coefficient measurements. The SWIR brightness values (SWIR brightness=brightness×(α/100); α=emission between 1,000–1,350 nm/total emission×100) followed a similar qualitative trend, yet benefit the micelles, FBS and EtOH by larger factors (~3-, ~9-, and ~14-fold, respectively), as these solvents have a larger fraction of total emission in the SWIR region compared to water. The emission ratio was calculated using the emission between 1,000–1,350 nm to approximate the SWIR region while avoiding interference from the doubling of the excitation wavelength at ~1,420 nm. This was deemed a good approximation as fluorescence beyond 1,350 nm was minimal in comparison to that of the shorter SWIR wavelengths.[18]

2.2. Comparison to Literature Values

Our measurements tend to agree with more recent literature values (see Table S1). In EtOH, the Φ_F value we measured (14%) corroborates the study by Rurack and Spieles,[46] while the ε we measured is slightly higher than the reported value. As sources for error in ε tend to underestimate the true value, this difference could be reasonably explained by differences in purity due to the batches or sources of ICG. In water, the Φ_F we measured (2.9%) agrees with two previous studies by Philip *et al.*[47] and Jin *et al.*,[48] and is only slightly less than Hoshi *et al.*[49] Particularly in water, solvent reabsorption effects may impact the accuracy of the Φ_F measurement.[46] The ε in water we measured was similar to the value reported by Carr *et al.*[18] The increased brightness of ICG in protein-containing media such as albumin solutions, serum, and blood is well-documented in many prior studies, due to binding with proteins present in these media.[50–51] The photophysical values we measured in FBS were in good agreement with the study by Obnisbi *et. al.*[39] which reported a very similar ε and a slightly lower Φ_F value (9%). Looking at measurements in similar media, Pauli *et al.*[52] found a slightly lower Φ_F value (8%) in bovine serum albumin (BSA). All previous Φ_F measurements in plasma[37–38] and human serum albumin (HSA)[44] were significantly lower, but two of these studies[37–38] used relative methods to DMSO at 13%[53] (more recent studies have characterized the Φ_F of ICG in DMSO by the absolute method to be between 22–26%.[46,54]) Taken together, our photophysical measurements align with the recent values taken in different solvents in several studies. Importantly, the measurements presented in this article are obtained by the same methods,

providing systematic photophysical measurements of ICG that are calibrated to each other. Moreover, these values take into account the 1–5% of the emission which is in the SWIR.[18]

For *in vivo* imaging applications, the photophysical measurements in blood or encapsulated in a delivery vehicle are the most relevant. These experiments can be challenging due to the high opacity, scattering, and absorption in blood, as well as variation in blood source and quality, which are potential causes for disparity between measurements. The sole literature value we found for the Φ_F of ICG in whole blood was reported in 1978 to be ~1.2%.[55] This is ~10-fold lower than the value we measured (13%); however, the reference value for the relative measurement is unclear. Nonetheless, in the same study, the Φ_F value reported in water was also ~10-fold lower than the value we measured here, indicating that the relative improvement between water and blood agrees in both studies. The value we measured in blood is close to the Φ_F in FBS, and is much higher than that measured in water, indicating that the emissive behavior in FBS likely approximates that of whole blood. Finally, the modest increase in quantum yield and brightness for ICG in micelles (~2–3 fold) compared to pure water is in line with previous findings in which ICG brightness increased upon encapsulation in a variety of structurally different micelles.[45,56–58]

2.3. High Concentration Photophysical Characterization

In the preceding section, we performed absorption measurements at low concentrations to ensure that ICG was present in its monomeric form. However, some imaging experiments, particularly photoacoustic imaging studies[18–20] are performed at high concentrations (~1 mM). Thus, it is useful to understand the photophysical behavior of ICG at higher concentrations, specifically, the roles of aggregation and self-quenching. Aggregation of ICG in solution can be observed by the increase of a blue shifted peak at ~700 nm (an H-aggregate) and a decrease of the monomeric peak at ~780–800 nm. Comparing the behavior in water to that in FBS, we found that in water, ICG begins to aggregate at concentrations as low as 10 μM. Aggregation intensifies with an increase in concentration, up to at least 500 μM (Figure S6). In contrast, FBS is able to solubilize ICG monomerically at higher concentrations, with only slight aggregation occurring at 500 μM and 1 mM. These results, which are in line with prior studies,[59] indicate that *in vivo* experiments at concentrations up to ~1 mM likely will not suffer from substantial aggregation of ICG. While aggregation is likely not a major factor *in vivo* at these concentrations, self-quenching (dye re-absorption of the emitted fluorescence signal) in fluorescence-based experiments remains a concern at high concentrations.[17] To determine the linearity bounds in our system, we examined the signal of ICG in capillary tubes at increasing concentrations in ethanol using a SWIR imaging configuration. We found that the signal from ICG increases linearly (R^2=0.95) from 1 μM to 50 μM (Figure S7). Thus, we employed concentrations within these bounds for further photophysical characterization using SWIR imaging. Similarly, for quantitative *in vivo* experiments, care should be taken to ensure that signal is linear over the studied concentration range.

2.4. Photostability

Photostability is a key characteristic for imaging agents, and becomes particularly relevant when imaging is performed over a long temporal period or high-powered light irradiation

is employed. Thus, photostability is a commonly compared property when evaluating chromophore performance. We examined the photostability of ICG in the selected solvents by irradiating samples of equal concentrations (5 μM) in capillary tubes with 785 nm excitation (119 $mWcm^{-2}$) and collecting the emission intensity over time (Table 1, Figure 2, Figure S8). ICG displayed the lowest photostability in water and the highest photostability in EtOH (improved by ~16-fold compared to water). Surprisingly, encapsulation in the PEG-lipid micelles did not offer an improvement in photostability compared to neat water. This observation is in contrast to findings by others, in which nanoparticle encapsulation, for example in poly(lactic-*co*-glycolic acid) polymer nanoparticles,[60] lipid-coated superparamagnetic iron oxide nanoparticles,[61] mesoporous silica nanoparticles,[62] and calcium phosphate nanoparticles,[63] have increased photostability compared to free ICG. The larger size and in some cases hard composition of these nanoparticles may offer more shielding from the aqueous environment and/or oxygen than the micelles observed here. In contrast, dissolution in whole blood and FBS improved the photostability of ICG compared to that in water by ~2-fold and ~4-fold, respectively. The high photostability of ICG in organic solvent compared to water is in agreement with previous observations,[64] although in the same study, human plasma was found to result in even higher photostability than the organic solvents methanol and DMSO. These results support that photostability measurements of ICG in water will likely show faster photobleaching than would occur *in vivo*.

2.5. SWIR Brightness Comparisons

Finally, we observed the SWIR emission of ICG in a SWIR imaging configuration and compared the brightness between the selected solvents. ICG was placed in capillary tubes at equal concentrations (5 μM) in the relevant solvents (Figure 3a), irradiated with 785 nm light (63 mW cm^{-2}) and the emission was observed with an InGaAs detector. Due to a small variation in laser irradiation over the area where tubes were imaged, we first measured the signal obtained from imaging with each tube positioned at all five locations in the capillary holder (Figure S9). From these images, we calculated the standard deviation between positions for each solvent, and applied these error values to the subsequent measurements. Next, we measured brightness values of the capillary tubes using 1,000 nm, 1,100 nm, and 1,300 nm longpass filtering (Figure 3b–d). Compared to water, the emission intensity in micelles, FBS, blood, and EtOH was higher by ~ 3-fold, ~ 10-fold, ~ 13-fold, and ~ 16-fold, respectively, using 1,000 nm longpass filtering. These ratios are similar to those obtained looking at the calculated SWIR brightness numbers in Table 1 for micelles, FBS, and EtOH. In blood, we observe slightly higher SWIR emission compared to FBS. This observation aligns well with the similar quantum yield measurements in blood and FBS (Table 1). Additionally, although we were unable to obtain a calculated SWIR brightness number for ICG in blood (due to high scattering in absorption measurements), the comparative brightness measurement allows us to infer that the absorption coefficient value of ICG in blood must be very similar, or slightly higher than that of FBS. Further, it allows us to arrive at estimated value for SWIR brightness, $\sim 4\times10^4$ using the relative performance of ICG in blood compared to water.

Moving to longer wavelengths of detection, the overall emission intensity decreases drastically (Figure 3e). Despite a decrease in signal, imaging with longer detection wavelengths have been shown to provide higher contrast of labelled biological structures.[18] The SWIR emission from ICG decreases by ~5 fold using detection with 1,100 nm longpass filtering and by ~70-fold using detection with 1,300 nm longpass filtering, compared to detection with 1,000 nm longpass filtering. Yet, the brightness between solvents remains relatively similar in each of these detection windows, indicating that the different solvent environments have minimal effects on the shape of the emission tail. Overall, the brightness measurements using an InGaAs detector show similar brightness differences between solvents compared to photophysical measurements and are independent of the longpass filter used.

3. Conclusion

From the measurements we report here, we find that solubilization in ethanol leads to the brightest solutions of ICG, and water significantly lowers brightness. Additionally, photobleaching occurs slowest in ethanol and fastest in water. A micellar formulation enhances the photophysical properties slightly from those measured in water. Moving to the biologically relevant media, we found that the photophysical behavior of ICG in whole blood and FBS is very similar and significantly brighter and more photostable than water. These differences in brightness are accentuated even more when only looking at SWIR wavelengths, where solutions in blood and FBS show between ~13 to ~16-fold higher emission than solutions in water, highlighting the necessity of performing comparative SWIR experiments in these media. With simpler storage conditions, easier handling and decreased scattering in FBS compared to blood, this medium could be an ideal alternative to blood for benchmarking studies for brightness and photostability. When aiming for a comparison which will represent biological performance, comparisons to ICG in water or similar media should be avoided as these media severely underestimate the ε, Φ_F, and photostability values that are present in biological media.

Experimental Section

Chemicals and materials

Indocyanine Green (ICG) was purchased from Acros Organics (IR-125, laser grade). Ethanol (EtOH) (200 Proof) was purchased from Decon Labs. MilliQ water was dispensed from a MilliQ water purification system. Fetal bovine serum (FBS) was purchased from Genesee Scientific (Lot no. P078430) and was not heat inactivated. Defibrinated Sheep Blood was purchased from Thermo Scientific (Remel sheep blood defibrinated, Ref. R54012, Lot 883930 and Lot 142514). The lipid 18:0 PEG2000 PE was purchased from Avanti Polar Lipids. All materials were used as received without further purification.

Micelle fabrication

ICG (0.6 mg, 0.77 μmol) was massed (Sartorius MSE6.6S-000-DM Cubis Micro Balance) and dissolved in 3.0 mL MeOH. A volume of 2.75 mL of the ICG solution was then added to 44.1 mg of 18:0 PEG2000 PE (as a powder). Of this solution, 0.5 mL aliquots were taken

into separate vials and evaporated on a rotary evaporator. To each vial, deionized water (5 mL) was added and the solution was sonicated in a bath sonicator for 1 minute.

Dynamic light scattering (DLS) measurements

Nanomaterial size was analyzed with a Malvern Zetaziser Nano dynamic light scattering in plastic 1 cm cuvettes. Samples were passed through a 0.22 μm cellulose acetate (CA) syringe filter, centrifuged at 6000 g for 20 minutes, passed through a second 0.22 μm CA syringe filter, and diluted 50-fold before measurement.

Absorption measurements

Absorption spectra were acquired on a JASCO V-770 UV-VIS/NIR spectrophotometer with a 2,000 nm/min scan rate after blanking with the appropriate solvent in quartz cuvettes (10 mm for measurements in EtOH, water, FBS, and micelles in water, 0.2 mm for measurements in whole blood).

Absorption coefficient measurements

Absorption coefficients were measured using serial dilutions with Hamilton syringes in volumetric glassware and are taken as the average ± standard deviation of 3 replicate measurements. See Figure S5 for the reported traces and Table 1 for the reported values. The apparent absorption coefficient measurement for ICG in phospholipid-PEG micelles was obtained by taking micelle solutions and measuring absorption spectra. The micelle solutions were then lyophilized, re-dissolved in EtOH and their absorption spectra were acquired. From the absorption spectra in EtOH, the concentration of each original micelle solution could be obtained using the ε value in EtOH and Beer's law ($A=\varepsilon lc$) Thus, knowing the absorbance (A), path length (l), and, concentration (c) of the micelle solution, an apparent absorption value (ε) was calculated. The apparent absorption coefficient value was reported as the average and standard deviation of 5 measurements.

Emission measurements

Photoluminescence spectra were obtained on a Horiba Instruments PTI QuantaMaster Series fluorometer with InGaAs detector Horiba Edison DSS IGA 020 L in quartz cuvettes (10 mm for measurements in EtOH, water, and micelles in water, 2 mm for measurements in FBS, and 0.2 mm for measurements in whole blood) with a 90° angle between excitation and detection. The whole blood samples in a 0.2 mm cuvette were positioned at a 45° angle to both the excitation and detection directions for front-facing collection in order to minimize scattering and reabsorption by the blood. The reported emission trace of ICG in whole blood was corrected by subtraction of the trace obtained using neat blood with identical acquisition conditions (Figure S4).

Quantum yield measurements

Absolute quantum yield measurements were taken in a Horiba KSPHERE-Petite integrating sphere on the Horiba Instruments fluorometer and are reported as the average ± standard deviation of 3 replicate measurements. For quantum yield measurements, samples were excited with 710 nm and collected between 730–1375 nm. Slit widths were 15 nm

excitation/ emission with 1 nm step size and 0.1 s integration time. The excitation light was collected between 680–740 nm. The spectra were corrected for excitation with the default correction file using a bias of −1.047, and emission, using a NIR correction file calibrated to quanta. Integrals were obtained for each of the traces, between 740–1375 for the dye emission and between 680–740 nm for the excitation light. Measurements in EtOH, water, micelles, and FBS were obtained in 10 mm×10 mm quartz cuvettes. Measurement in blood was obtained in a 10 mm×2 mm quartz cuvette. Optical densities of all samples were below 0.1 to minimize effects of reabsorption. See Table 1 for the reported quantum yield values.

Aggregation studies

1 mM solutions of ICG were prepared in milliQ water or FBS and serial dilutions were performed to obtain solutions of varying concentrations between 1 mM and 1 uM. To accommodate the large range in absorbances, cuvettes with three different path lengths were used for absorption measurements (0.2 mm, 3 mm, and 10 mm). The absorbance traces were normalized to the highest peak, either the aggregate peak at 697 nm or the monomer peak at 792 nm (FBS) or 778 nm (water) and displayed in Figure S6.

SWIR imaging apparatus

An InGaAs Camera (Allied Vision Goldeye G-032 Cool TEC2) camera was fitted with a C-mount camera lens (Kowa LM35HC-SW) and variable emission filters as defined in each experiment and mounted vertically above an imaging workspace. The camera used a sensor temperature set point of −30 °C. The “785” laser (LUMICS, LU0785DLU250-S70AN03, specified to an error of ± 10 nm) output was coupled cube via a 600 nm core fiber-optic bundle (Lumics, LU_LWL0600_0720_220D1A1). The output from the fiber was fixed in an excitation cube (Thorlabs KCB1E), reflected off of a mirror (Thorlabs BBE1-E03), and passed through a positive achromat (Thorlabs AC254-050-AB-ML), 2×1,000 nm short-pass filters (Edmund Optics #64–337) and an engineered diffuser (Thorlabs ED1-S20-MD) to provide uniform illumination over the working area. The excitation flux was measured over the area of interest with a digital optical power and energy meter (Thorlabs PM100D, specified to an error of ± 3%) and the values over the imaging area were averaged to reach the reported number. The assembly was partially enclosed to avoid excess light while enabling manipulation of the field of view during operation. Camera and lasers were externally controlled and synchronized by delivering trigger pulses of 5 V Transistor-Transistor Logic to the laser drivers and camera using a programmable trigger controller with pulses generated with an Atmel Atmega328 micro-controller unit and programmed using Arduino Nano Rev 3 MCU (A000005) in the Arduino integrated development environment (IDE). Acquired imaging data is then transferred to the PC via a Gigabit Ethernet interface. For image acquisition, the toolbox of MATLAB programming environment was used in combination with a MATLAB script (CCDA V3, https://gitlab.-com/brunslab/ccda) to preview and collect the required image data in 14-bit depth. Images were processed using the FIJI distribution of ImageJ.

Photobleaching experiments

Solutions of ICG in each media were prepared and diluted to 5 μM by serial dilutions using micropipettes. Solutions were drawn up into capillary tubes (Corning, 100 μL) and placed

in a capillary holder for alignment. Images were acquired of three capillary tube samples using 1,100 nm LP filtering (2× 1,000 nm and 1× 1,100 nm LP filters were used: FELH 1000 (Thorlabs), #84–766 (Edmund Optics), #84–768 (Edmund Optics)). Solutions were irradiated with the 785 nm laser (119 mW cm^{-2}) and images were collected at 1 fps with variable exposure times depending on the brightness of the sample (EtOH=2 ms, water=20 ms, micelles=10 ms, FBS=3 ms, blood=2 ms). Images were background corrected, and a region of interest (ROI) was drawn over each tube. The normalized average intensity and standard deviation of the three trials are plotted in Figure 2. All photobleaching data were fit to a mono-exponential decay (Figure S8) and the rate constants were obtained from the first order reaction equation [Eq. (1)]:

$$\ln[A] = -kt + \ln[A]_o \quad (1)$$

where A and A_o represent the emission collected at time t and the initial emission collected, respectively. All R^2 values were >0.96. The photobleaching rates (k_{raw}) are reported in Table 1. Relative photostability values (Table 1) were obtained by taking the ratio of the k_{raw} in water over the k_{raw} in the relevant solvent.

Brightness experiments

Solutions of ICG in each media were prepared and diluted to 5 μM by serial dilutions using micropipettes. Solutions were drawn up into capillary tubes (Corning, 100 μL) and placed in a capillary holder for alignment. Solutions were irradiated with the 785 nm laser (63 mW cm^{-2}) and images were collected with either 1,000 nm filtering (3× 1,000 nm LP filters were used: FELH 1000 (Thorlabs), 2× #84–766 (Edmund Optics)), 1,100 nm filtering (2× 1,000 nm and 1× 1,100 nm LP filters were used: FELH 1000 (Thorlabs), #84–766 (Edmund Optics), #84–768 (Edmund Optics)), or 1,300 nm filtering (2× 1,000 nm and 1 × 1,300 nm LP filters were used: FELH 1000 (Thorlabs), #84–766 (Edmund Optics), #88–668 (Edmund Optics)). Frame rates and exposure times were variable depending on the brightness of the samples in the optical configuration (1,000 LP=1 ms; 1,100 LP=5 ms; 1,300 LP=40 ms). Images were background subtracted, Z-averaged over 100 frames, rotated 90° clockwise, and cropped. The contrast was set in the 14-bit image and the minimum and maximum intensity values were recorded and are displayed in the legend next to each image (Figure 3b–d) before converting the file to 8-bit for display. The look-up table LUT CET–L16 was used for display. The profiles were obtained by analyzing the plot profile over a rectangular area (averaging signal in the Y-dimension to display a single curve). The column graph (Figure 3e) was constructed using the highest value over each capillary tube and the error as measured in control experiments (Figure S9).

Supplementary Material

Refer to Web version on PubMed Central for supplementary material.

Acknowledgements

We thank the NSF (NSF GFRP DGE-1144087 to E.D.C), the NIH (1R01EB027172 to E.M.S.), the Foote Family (E.D.C.), the Alfred P. Sloan Foundation (FG-2018-10855 to E.M.S.) and UCLA for financial support. We thank Dr. Laurent Bentolila for discussion and support in building the SWIR imaging apparatus at the Advanced

Light Microscopy/Spectroscopy Laboratory (ALMS) at the California NanoSystems Institute at UCLA. Additional thanks to Dr. Oliver Bruns and Martin Warmer (Helmholtz Pioneer Campus (HPC)) for guidance in building the SWIR imaging apparatus. ALMS is supported in part with funding from NIH Shared Instrumentation Grant S10OD025017 and NSF Major Research Instrumentation grant CHE-0722519. NMR spectra were obtained on an instrument purchased via shared instrumentation grant from the NIH (1S10OD016387). We thank Duilio Cascio (UCLA) for 3D printing, Peter Tsrunchev (HPC) for software assistance, and Prof. Justin Caram (UCLA), Bernardo Arús (HPC) and Jakob Lingg (HPC) for critical reading of this manuscript.

References

[1]. Marshall MV, Rasmussen JC, Tan I, Aldrich MB, Adams KE, Wang X, Fife CE, Maus EA, Smith LA, Sevick-Muraca EM, Open Surg. Oncol. J2010, 2, 12–25. [PubMed: 22924087]

[2]. Tozzi M, Boni L, Soldini G, Franchin M, Piffaretti G, Case Rep. Transplant2014, 2014, 1–5.

[3]. Rasmussen JC, Tan I, Marshall MV, Fife CE, Sevick-Muraca EM, Curr. Opin. Biotechnol2009, 20, 74–82. [PubMed: 19233639]

[4]. Kwon S, Sevick-Muraca EM, Immunol J. Methods2010, 360, 167–172.

[5]. Rasmussen JC, Fife CE, Sevick-Muraca EM, Lymphatic Res. Biol2015, 13, 195–201.

[6]. Cousins A, Thompson SK, Wedding AB, Thierry B, Biotechnol. Adv2014, 32, 269–279. [PubMed: 24189095]

[7]. De Gasperi A, Mazza E, Prosperi M, World JHepatol2016, 8, 355–367.

[8]. Schwarz C, Plass I, Fitschek F, Punzengruber A, Mittlböck M, Kampf S, Asenbaum U, Starlinger P, Stremitzer S, Bodingbauer M, Kaczirek K, Sci. Rep2019, 9, 1–7. [PubMed: 30626917]

[9]. Kwon S, Sevick-Muraca EM, Neurogastroenterol. Motil2011, 23, 881–e344. [PubMed: 21624010]

[10]. Li Z, Yao S, Xu J, Wu Y, Li C, He Z, Ann. N. Y. Acad. Sci2018, 1421, 88–96. [PubMed: 29740828]

[11]. Velde EA, Veerman T, Subramaniam V, Ruers T, te Velde EA, Veerman T, Subramaniam V, Ruers T, Eur. J. Surg. Oncol2010, 36, 6–15. [PubMed: 19926438]

[12]. Polom K, Murawa D, Rho Y.-s., Nowaczyk P, Hunerbein M, Murawa P, Cancer2011, 117, 4812–4822. [PubMed: 21484779]

[13]. Schaafsma BE, Mieog JSD, Hutteman M, van der Vorst JR, Kuppen PJK, Lowik CWGM, Frangioni JV, van de Velde CJH, Vahrmeijer AL, J. Surg. Oncol2011, 104, 323–332. [PubMed: 21495033]

[14]. Daskalaki D, Fernandes E, Wang X, Bianco FM, Elli EF, Ayloo S, Masrur M, Milone L, Giulianotti PC, Surg. Innov2014, 21, 615–621. [PubMed: 24616013]

[15]. Koch M, Ntziachristos V, Annu. Rev. Med2016, 67, 153–164. [PubMed: 26768238]

[16]. Yim JJ, Tholen M, Klaassen A, Sorger J, Bogyo M, Mol. Pharm2017, 15, 750–758. [PubMed: 29172524]

[17]. Gioux S, Choi HS, Frangioni JV, Mol. Imaging2010, 9, 237–255. [PubMed: 20868625]

[18]. Okumura K, Yoshida K, Yoshioka K, Aki S, Yoneda N, Inoue D, Kitao A, Ogi T, Kozaka K, Minami T, Koda W, Kobayashi S, Takuwa Y, Gabata T, Eur. Radiol. Exp2018, 2, 5. [PubMed: 29708213]

[19]. Capozza M, Blasi F, Valbusa G, Oliva P, Cabella C, Buonsanti F, Cordaro A, Pizzuto L, Maiocchi A, Poggi L, Photoacoustics2018, 11, 36–45. [PubMed: 30105205]

[20]. Chaudhary Z, Khan GM, Abeer MM, Pujara N, Wan-Chi Tse B, McGuckin MA, Popat A, Kumeria T, Biomater. Sci2019, 7, 5002–5015. [PubMed: 31617526]

[21]. Carr JA, Franke D, Caram JR, Perkinson CF, Saif M, Askoxylakis V, Datta M, Fukumura D, Jain RK, Bawendi MG, Bruns OT, Proc. Nat. Acad. Sci2018, 115, 4465–4470. [PubMed: 29626132]

[22]. Starosolski Z, Bhavane R, Ghaghada KB, Vasudevan SA, Kaay A, Annapragada A, PLoS One2017, 12, e0187563. [PubMed: 29121078]

[23]. Yu X, Feng Z, Cai Z, Jiang M, Xue D, Zhu L, Zhang Y, Liu J, Que B, Yang W, Xi W, Zhang D, Qian J, Li G, J. Mater. Chem. B2019, 7, 6623–6629. [PubMed: 31591622]

[24]. Cai Z, Zhu L, Wang M, Roe AW, Xi W, Qian J, Theranostics2020, 10, 4265–4276. [PubMed: 32226552]

[25]. Li Z, Zaid W, Hartzler T, Ramos A, Osborn ML, Li Y, Yao S, Xu J, Ann. N. Y. Acad. Sci2019, 1448, 42–51. [PubMed: 30951208]

[26]. Cosco ED, Spearman AL, Ramakrishnan S, Lingg JGP, Saccomano M, Pengshung M, Arús BA, Wong KCY, Glasl S, Ntziachristos V, Warmer M, McLaughlin RR, Bruns OT, Sletten EM, Nat. Chem2020, 12, 113–1130. [PubMed: 31996808]

[27]. Cosco ED, Arús BA, Spearman AL, Atallah TL, Lim I, Leland OS, Caram JR, Bischof TS, Bruns OT, Sletten EM, J. Am. Chem. Soc2021, 143 (18), 6836–6846. [PubMed: 33939921]

[28]. Hu Z, Fang C, Li B, Zhang Z, Cao C, Cai M, Su S, Sun X, Shi X, Li C, Zhou T, Zhang Y, Chi C, He P, Xia X, Chen Y, Gambhir SS, Cheng Z, Tian J, Nat. Biomed. Eng2020, 4, 259–271. [PubMed: 31873212]

[29]. Patel NJ, Manivannan E, Joshi P, Ohulchanskyy TJ, Nani RR, Schnermann MJ, Pandey RK, Photochem. Photobiol2015, 91, 1219–1230. [PubMed: 26108696]

[30]. Wang S, Fan Y, Li D, Sun C, Lei Z, Lu L, Wang T, Zhang F, Nat. Commun2019, 10, 1058. [PubMed: 30837470]

[31]. Zhu S, Hu Z, Tian R, Yung BC, Yang Q, Zhao S, Kiesewetter DO, Niu G, Sun H, Antaris AL, Chen X, Adv. Mater2018, 30, 1802546.

[32]. Lei Z, Sun C, Pei P, Wang S, Li D, Zhang X, Zhang F, Angew. Chem. Int. Ed2019, 58, 8166–8171; *Angew. Chem.***2019**, *131*, 8250–8255.

[33]. Li B, Zhao M, Feng L, Dou C, Ding S, Zhou G, Lu L, Zhang H, Chen F, Li X, Li G, Zhao S, Jiang C, Wang Y, Zhao D, Cheng Y, Zhang F, Nat. Commun2020, 11, 3102. [PubMed: 32555157]

[34]. Byrd BK, Folaron MR, Leonor JP, Strawbridge RR, Cao X, Bruza P, Davis SC, J. Biomed. Opt2019, 24, 1.

[35]. Shi Y, Yuan W, Liu Q, Kong M, Li Z, Feng W, Hu K, Li F, ACS Materials Lett2019, 1, 418–424.

[36]. Ding B, Xiao Y, Zhou H, Zhang X, Qu C, Xu F, Deng Z, Cheng Z, Hong X, J. Med. Chem2019, 62, 2049–2059. [PubMed: 30501190]

[37]. Feng Z, Yu X, Jiang M, Zhu L, Zhang Y, Yang W, Xi W, Li G, Qian J, Theranostics2019, 9, 5706–5719. [PubMed: 31534513]

[38]. Tian R, Ma H, Zhu S, Lau J, Ma R, Liu Y, Lin L, Chandra S, Wang S, Zhu X, Deng H, Niu G, Zhang M, Antaris AL, Hettie KS, Yang B, Liang Y, Chen X, Adv. Mater2020, 32, 1–10.

[39]. Mangold K, Shaw JA, Vollmer M, Eur. J. Phys2013, 34, S51–S71.

[40]. Licha K, Riefke B, Semmler W, Proc. SPIE1996, 2927, 192–198.

[41]. Licha K, Riefke B, Ntziachristos V, Becker A, Chance B, Semmler W, Photochem. Photobiol2000, 72, 392. [PubMed: 10989611]

[42]. Obnisbi S, Lomnes SJ, Laurence RG, Gogbasbian A, Mariant G, Frangioni JV, Mol. Imaging2005, 4, 172–181. [PubMed: 16194449]

[43]. Egloff-Juras C, Bezdetnaya L, Dolivet G, Lassalle HP, Int. J. Nanomed2019, 14, 7823–7838.

[44]. Landsman ML, Kwant G, Mook GA, Zijlstra WG, J. Appl. Physiol1976, 40, 575–583. [PubMed: 776922]

[45]. Bhavane R, Starosolski Z, Stupin I, Ghaghada KB, Annapragada A, Sci. Rep2018, 8, 14455. [PubMed: 30262808]

[46]. Rurack K, Spieles M, Anal. Chem2011, 83, 1232–1242. [PubMed: 21250654]

[47]. Philip R, Penzkofer A, Baumler W, Szeimies RM, Abels C, J. Photochem. Photobiol. A1996, 96, 137–148.

[48]. Jin T, Tsuboi S, Komatsuzaki A, Imamura Y, Muranaka Y, Sakata T, Yasuda H, MedChemComm2016, 7, 623–631.

[49]. Hoshi R, Suzuki K, Hasebe N, Yoshihara T, Tobita S, Anal. Chem2020, 92, 607–611. [PubMed: 31769292]

[50]. Mordon S, Devoisselle JM, Soulie-Begu S, Desmettre T, Microvasc. Res1998, 55, 146–152. [PubMed: 9521889]

[51]. Jung Bongsu, Vullev VI, Anvari B, IEEE J. Sel. Top. Quantum Electron2014, 20, 149–157.

[52]. Pauli J, Brehm R, Spieles M, Kaiser WA, Hilger I, Resch-Genger U, J. Fluoresc2010, 20, 681–693. [PubMed: 20213244]

[53]. Benson RC, Kues HA, J. Chem. Eng. Data1977, 22, 379–383.

[54]. Würth C, Pauli J, Lochmann C, Spieles M, Resch-Genger U, Anal. Chem2012, 84, 1345–1352. [PubMed: 22242570]

[55]. Benson RC, Kues HA, Phys. Med. Biol1978, 23, 159–163. [PubMed: 635011]

[56]. Kirchherr AK, Briel A, Mäder K, Mol. Pharm2009, 6, 480–491. [PubMed: 19228053]

[57]. Kim TH, Chen Y, Mount CW, Gombotz WR, Li X, Pun SH, Pharm. Res2010, 27, 1900–1913. [PubMed: 20568000]

[58]. Meyer J, Cunea A, Sonntag-Bensch D, Welker P, Licha K, Holz FG, Schmitz-Valckenberg S, Invest. Ophthalmol. Visual Sci2014, 55, 6204–6212. [PubMed: 25190666]

[59]. Zhou JF, Chin MP, Schafer SA, Proc. SPIE1994, 2128, 495–505.

[60]. Saxena V, Sadoqi M, Shao J, J. Photochem. Photobiol. B2004, 74, 29–38. [PubMed: 15043844]

[61]. Ma Y, Tong S, Bao G, Gao C, Dai Z, Biomaterials2013, 34, 7706–7714. [PubMed: 23871538]

[62]. Sharma P, Bengtsson NE, Walter GA, Sohn HB, Zhou G, Iwakuma N, Zeng H, Grobmyer SR, Scott EW, Moudgil BM, Small2012, 8, 2856–2868. [PubMed: 22744832]

[63]. Altinog˘lu EI, Russin TJ, Kaiser JM, Barth BM, Eklund PC, Kester M, Adair JH, ACS Nano2008, 2, 2075–2084. [PubMed: 19206454]

[64]. Holzer W, Mauerer M, Penzkofer A, Szeimies R-M, Abels C, Landthaler M, Bäumler W, J. Photochem. Photobiol. B1998, 47, 155–164. [PubMed: 10093915]

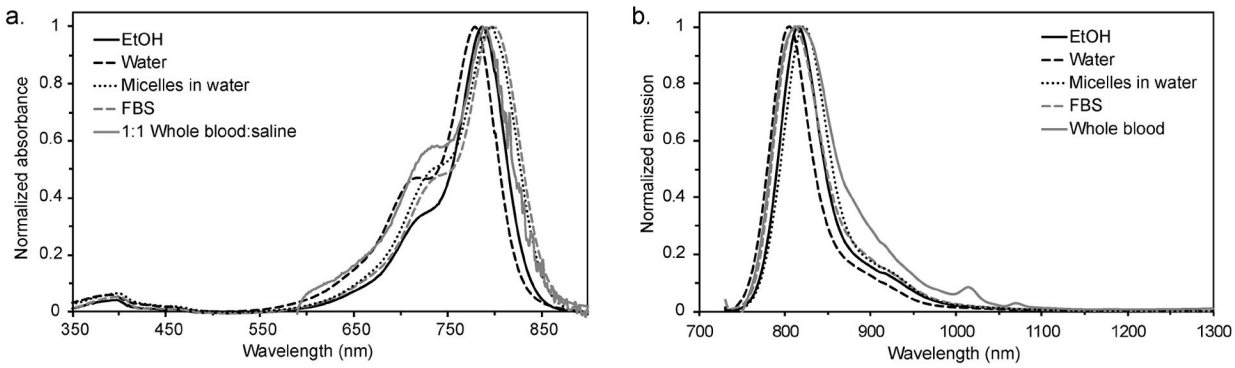

Figure 1.

Absorption (a) and emission (b) (excitation: 710 nm) of ICG in various media. See Figure S4 for correction of the emission trace in blood.

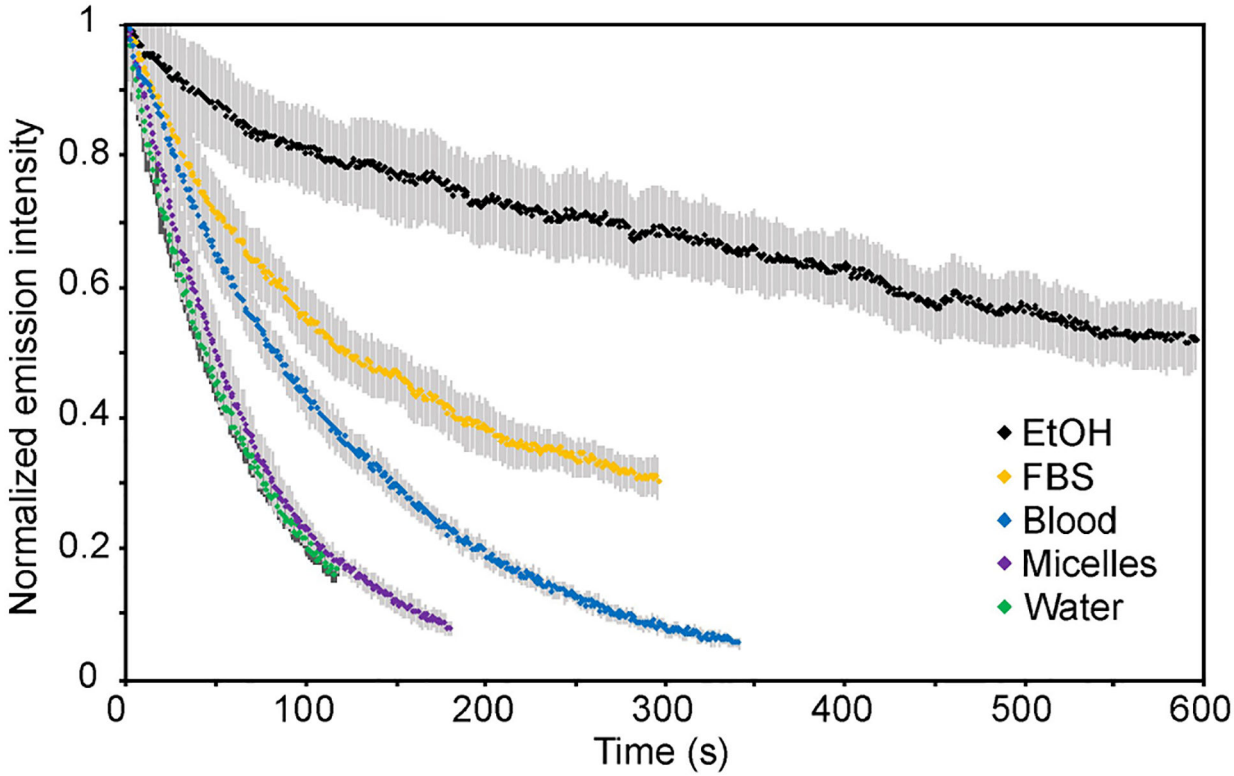

Figure 2.

Photostability of ICG in different solvents. Samples in capillary tubes were irradiated with 785 nm (119 $mWcm^{-2}$) light and their emission (longpass 1100 nm) was measured on an InGaAs detector. Intensity is graphed as the percent initial emission. Error is displayed as the standard deviation of the triplicate measurement.

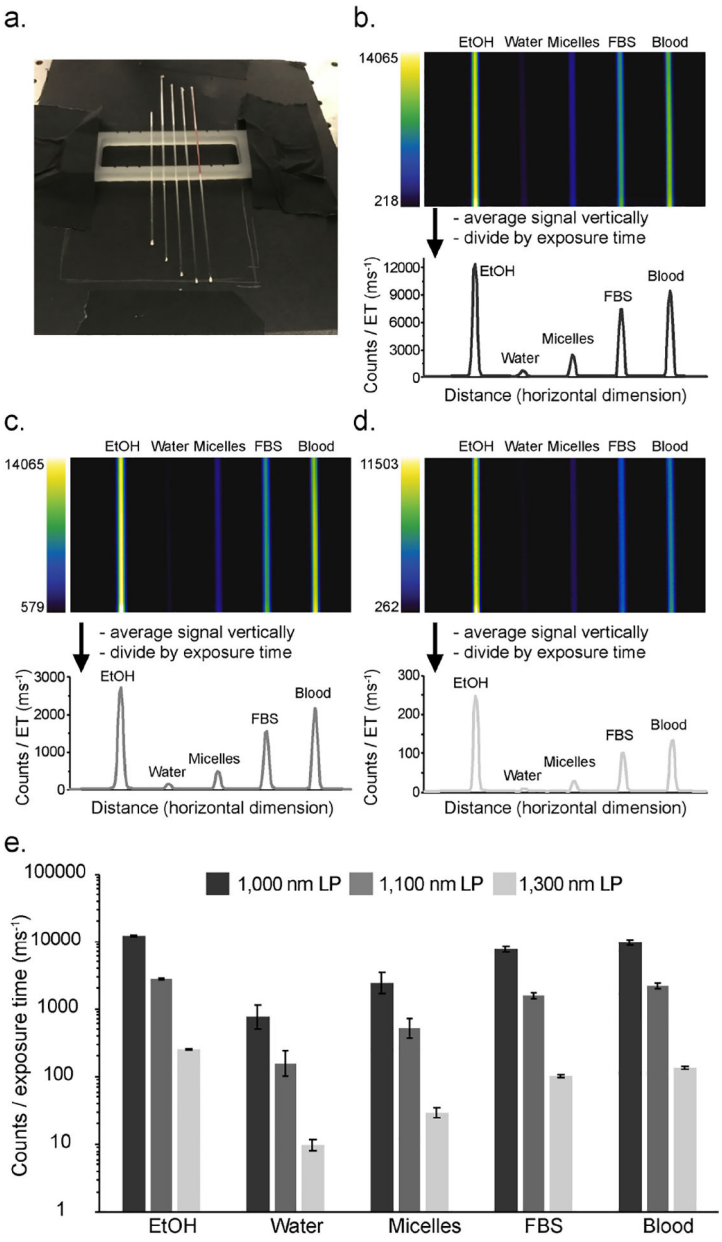

Figure 3.

SWIR brightness comparison of ICG emission in various solvents. a) Visible photograph of capillary tubes and holder used in imaging experiment. b–d) Images of capillary tubes and graphical profiles of emission intensity using 785 nm irradiation (63 $mWcm^{-2}$) with 1,000 nm [(b) 1 ms ET], 1,100 nm [(c) 5 ms ET], and 1,300 nm [(d) 40 ms ET] longpass filtering. All emission intensities displayed in the graphs were corrected for exposure time (ET) differences. e) Quantification of emission intensity compared between solvents and longpass filter wavelengths. Error is estimated from a separate experiment (see Figure S7), which quantifies variation in emission intensity (as the standard deviation) due to positioning of the capillary tube in relation to the laser irradiation profile.

Table 1.

Photophysics of ICG in various media.

Solvent	$\lambda_{max,abs}$ [nm]	ε [M^{-1} cm^{-1}]	$\lambda_{max,em}$ [nm]	Φ_F [%]	Brightness[g] ×10^4 [M^{-1} cm^{-1}]	SWIR emission, α[h] [%]	SWIR brightness[i] ×10^4 [M^{-1} cm^{-1}]	Photobleaching rate k_{raw}×10^3 [s^{-1}]	Relative photostability
EtOH	787	223 000 ± 6 000	815	14 ± 1	310 ± 20	1.44	4.5 ± 0.3	0.98 ± 0.09	16 ± 1
Water	779	156 000 ± 6 000	805	2.9 ± 0.2	45 ± 4	0.71	0.32 ± 0.03	15.5 ± 0.2	1
FBS[a]	798	162 000 ± 3 000	811	12.0 ± 0.9	190 ± 20	1.43	2.8 ± 0.2	3.85 ± 0.05	4.03 ± 0.06
Micelles[b]	796	180 000± 8 000[e]	821	5.1 ± 0.3	92 ± 7	0.99	0.91 ± 0.07	14.2 ± 0.4	1.09 ± 0.03
Whole blood[c]	788[d]	n.r.[f]	815	13 ± 1	n.r.	5.15	n.r.	8.4 ± 0.3	1.84 ± 0.06

[a] FBS=Fetal bovine serum.

[b] 18:0 PEG2000 PE micelles dispersed in water.

[c] Defibrillated sheep blood.

[d] 1:1 whole blood:saline was used due to high scattering in whole blood.

[e] An apparent absorption coefficient is used, as described in the experimental procedures.

[f] High scattering prevented absorption coefficient measurements in this media.

[g] Brightness=$\varepsilon \times \Phi_F$.

[h] SWIR emission (α); α=emission between 1,000–1,350 nm/total emission×100.

[i] SWIR brightness=brightness×(α/100).

ChemPhotoChem. Author manuscript; available in PMC 2022 August 01.